PCCP

PAPER

View Article Online
View Journal | View Issue

Check for updates

Cite this: *Phys. Chem. Chem. Phys.*, 2018, **20**, 10155

Experimental evidence of TICT state in 4-piperidinyl-1,8-naphthalimide – a kinetic and mechanistic study

Zoltán Szakács,[a] Sylvia Rousseva,[a] Márton Bojtár,[b] Dóra Hessz,[c] István Bitter,[b] Mihály Kállay,[d] Michiel Hilbers,[e] Hong Zhang[e] and Miklós Kubinyi*[ac]

Received 21st December 2017,
Accepted 21st March 2018

DOI: 10.1039/c7cp08555a

rsc.li/pccp

The excited state processes in *N*-propyl-4-piperidinyl-1,8-naphthalimide have been studied by measuring its fluorescence spectra and decay curves in solvents of different polarity and viscosity and also in a frozen solvent glass. The results unanimously proved the formation of a dark twisted intramolecular charge transfer (TICT) state from the emissive charge transfer (CT) species, the direct product of excitation. The rate coefficients of the TICT process and the deactivations of the CT and TICT species were determined, using a reversible two-state kinetic model. The temperature dependence of the kinetic data was consistent with a kinetic barrier consisting of three terms, the inherent barrier of the reaction, and the contributions of the solute–solvent interactions related to the solvent viscosity and polarity. The potential energy surfaces were calculated in the S_0 and the S_1 states along the coordinate of turning motion which was conclusive concerning the direction of the twisting and indicated a possible conformational change of the piperidinyl unit. The theoretical calculations confirmed that the TICT species is dark and has a stronger charge transfer character compared to the CT state.

Open Access Article. Published on 28 March 2018. Downloaded on 2/9/2026 10:35:42 PM.
This article is licensed under a Creative Commons Attribution 3.0 Unported Licence.

Introduction

1,8-Naphthalimides (NIs) with an electron donor substituent in the 4-position, constitute an important class of push–pull type fluorescent compounds. Their fluorescence wavelengths and in particular, their fluorescence quantum yields are sensitive to the local environment. This attractive feature led to numerous naphthalimide-based fluorescent probes and chemosensors[1,2] for various cations,[3,4] anions,[5] small biomolecules[6,7] and protein–protein interactions.[8,9]

The parent compound, 1,8-naphthalimide, and its derivatives with weak donor/acceptor substituents exhibit low fluorescence quantum yields in apolar solvents, somewhat higher values in polar aprotic solvents, which increase further in protic solvents. The effect is due to an efficient intersystem crossing between their S_1 and T_2 excited states, lying close in apolar media. The interactions with polar, and in particular, with hydrogen-bond donor solvents shift the T_2 state to higher, the S_1 state to lower energies, reducing the effect.[10]

Introducing an electron donor substituent into the 4-position of 1,8-NI, the longest wavelength absorption and fluorescence bands are shifted to longer wavelengths.[11–14] In most cases, the fluorescence quantum yield becomes higher, because, with the lowering of the energy of the S_1 state, the S_1–T_2 energy gap becomes larger, reducing the yield of inter-system crossing.[11,13] The excitation is accompanied by an intramolecular charge transfer (CT) – an electron transfer from the substituent to the electron withdrawing dicarboximide group.[15] The excited species are stabilized by polar and more efficiently by protic polar solvents, as indicated by the redshift of the fluorescence band in polar media. The photogenerated higher electric field can serve for a fluorescence quenching mechanism which is called generally as photoinduced electron (charge) transfer (PET) in the literature.[16] This phenomenon is of key importance in the construction of NI-based 'turn-on' fluorescent chemosensors.[17] Most frequently, they contain an electron rich receptor unit attached through a spacer to their 4-position, or an electron withdrawing receptor unit connected through a spacer to their imide nitrogen atom. Their fluorescence quenched strongly in free state *via* PET mechanism, is restored when the analyte binds to the receptor unit, shielding its local charge.[2]

[a] *Department of Physical Chemistry and Materials Science, Budapest University of Technology and Economics, 1521 Budapest, Hungary. E-mail: kubinyi@mail.bme.hu*
[b] *Department of Organic Chemistry and Technology, Budapest University of Technology and Economics, 1521 Budapest, Hungary*
[c] *Institute of Materials and Environmental Chemistry, Research Center for Natural Sciences, Hungarian Academy of Sciences, P.O. Box 286, 1519 Budapest, Hungary*
[d] *MTA-BME Lendület Quantum Chemistry Research Group, Department of Physical Chemistry and Materials Science, Budapest University of Technology and Economics, 1521 Budapest, Hungary*
[e] *Van't Hoff Institute for Molecular Sciences, University of Amsterdam, P.O. Box 94157, 1090 GD Amsterdam, The Netherlands*

Open Access Article. Published on 28 March 2018. Downloaded on 2/9/2026 10:35:42 PM.
This article is licensed under a Creative Commons Attribution 3.0 Unported Licence.

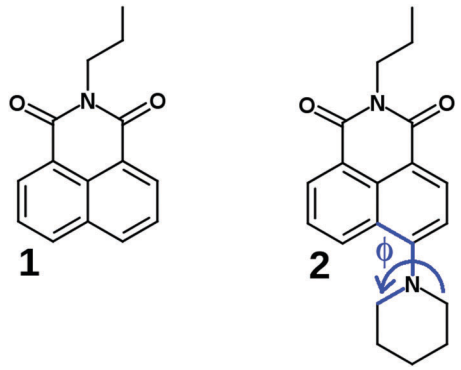

Fig. 1 The investigated compounds **1** and **2**, Φ is the fixed dihedral angle in the computational TICT study.

In NIs with more rigid electron donating groups on their 4-carbon atom, a twisted intramolecular charge transfer (TICT) process has also been discovered.[18] The TICT state may be emissive, manifesting in a dual fluorescence. Examples for this are NIs with a styrene or phenoxy unit inserted between an electron donor group and their 4-position.[19,20] More frequently, however, the TICT state is dark, leading only to the weakening of the emission from the CT excited state.[21] The TICT of push–pull NIs is of significance in several potential applications, like when these molecules act as polarity[8,9] and viscosity probes,[22] the inhibition of TICT in solid state leads to aggregation induced emission,[23–26] TICT and *E*/*Z* isomerization may occur as simultaneous reactions.[19]

Despite the fluorescence properties of several NIs have been interpreted in terms of two (a CT and a TICT) interconverting S_1 excited states, a comprehensive photophysical study had lacked on a more simple push–pull derivative to give experimental proof of the formation of TICT state. This motivated us to provide a detailed description of the excited state processes in *N*-propyl-4-piperidinyl-1,8-naphthalimide (**2**, see Fig. 1), combining experimental and theoretical methods. *N*-Propyl-1,8-naphthalimide (**1**) was used as reference compound. The rate coefficients of the reversible CT → TICT conversion were determined in different solvents at different temperatures, and were interpreted applying a kinetic barrier consisting of three terms, the inherent barrier of the reaction, and the contributions of the solvent viscosity and solvent polarity. The potential energy surfaces in the S_0 and S_1 states were calculated, along the coordinate of the turning motion which was conclusive concerning the direction of the twisting. The theoretical calculations confirmed a more efficient charge transfer of the dark TICT state compared to the CT state.

Experimental section

General

1 and **2** were prepared as described elsewhere.[27,28] Acetonitrile (MeCN), propionitrile (EtCN), butyronitrile (PrCN), valeronitrile (BuCN), caprylonitrile (HepCN), ethylene glycol (EG), methanol (MeOH) and ethanol (EtOH) solvents were purchased from Sigma Aldrich. MeCN was HPLC grade, MeOH and EtOH were spectroscopy grade and they were used without further purification. The other nitriles and the ethylene glycol were used after column chromatography purification using a mixed stationary phase (aluminium oxide 'Alumina B' and activated carbon) to remove the luminescent impurities.

Spectroscopic experiments

Absorption spectra were recorded using an Agilent 8453 diode array spectrometer. The steady state fluorescence spectra were measured on an Edinburgh Instruments FLS920 instrument, the recorded spectra were corrected with the characteristic of the light source and the detector. Time-resolved fluorescence experiments were performed using the frequency-doubled output of a Ti:sapphire laser system (Chameleon Ultra, Coherent) tuned to 820 nm and 700 nm which results in 410 nm and 350 nm excitation wavelengths for **2** and **1**, respectively. A pulse picker was employed to reduce the repetition rate from 80 to 8 MHz. The fluorescence was detected using a monochromator (Newport CS260-02) coupled to a PMT (Hamamatsu). The overall instrument response function (IRF) was ~20–25 ps (fwhm). A thermostated sample holder was used for the temperature dependent experiments in EG and a liquid nitrogen cryostat was used for the measurements at 77 K in frozen solvent glass (EtOH : MeOH, 4 : 1). All the experiments were performed at a concentration of 10 μM in 1 × 1 cm quartz cuvettes.

Methods

Dipole moment change

The dipole moment changes were determined from the absorption and fluorescence spectral data obtained in alkyl nitrils, using the Lippert–Mataga equation,[29,30]

$$\Delta\tilde{\nu} = \tilde{\nu}_a - \tilde{\nu}_{fl} = \frac{2 \cdot \Delta f \cdot (\mu_g - \mu_e)^2}{4 \cdot \pi \cdot \varepsilon_0 \cdot h \cdot c \cdot {a_0}^3} + C \qquad (1)$$

where $\tilde{\nu}_a$ and $\tilde{\nu}_{fl}$ are the wavenumbers of absorption and fluorescence maxima, μ_g and μ_e are the dipole moments in the ground and excited states – μ_g was calculated at the DFT level (for details see Computational section) – ε_0 is the vacuum permittivity, h is the Planck constant, c is the velocity of light, a_0 is the radius of the Onsager cavity. a_0 was also determined by quantum chemical calculations, it was taken as the sphere equivalent radius of the volume inside a contour of 0.001 electrons per Bohr^3 density plus 0.5 Angström (this is the recommended radius for self consistent reaction field (SCRF) calculations).[31] C in eqn (1) is a fitted constant, Δf is the orientation polarizability,

$$\Delta f = \frac{\varepsilon_r - 1}{2 \cdot \varepsilon_r + 1} - \frac{n^2 - 1}{2 \cdot n^2 + 1}, \qquad (2)$$

where ε_r is the dielectric permittivity, n is the refractive index of the medium.

Open Access Article. Published on 28 March 2018. Downloaded on 2/9/2026 10:35:42 PM.
This article is licensed under a Creative Commons Attribution 3.0 Unported Licence.

Quantum yield determination

The fluorescence quantum yields of NIs were determined using quinine sulfate (in 0.1 M H_2SO_4) as reference, applying the formula[32]

$$\Phi_{NI} = \Phi_{ref}\frac{\int I_{NI}(\tilde{\nu})d\tilde{\nu}}{\int I_{ref}(\tilde{\nu})d\tilde{\nu}}\frac{{n_{org}}^2}{{n_{water}}^2}\frac{A_{ref}}{A_{NI}} \quad (3)$$

The quantum yield of quinine sulfate, Φ_{ref} is 0.53 [33] the subsequent fractionals in eqn (3) are the ratios of the integrated fluorescence intensities, the refractive indices and the absorbances, the latter at the excitation wavelength.

Theoretical calculations

Theoretical calculations were performed to investigate the TICT process and to calculate the Onsager radius of NIs using the Gaussian09 program package.[31] The minimal-energy geometries were created in three steps. Firstly, we carried out a conformational analysis using the Merck molecular force field (MMFF94) with the Marvin Beans program package.[34] Secondly, the geometries with up to 8 kJ mol^{-1} from the lowest energy conformer were optimized using PM6-D3H4 (parametrized model 6 with dispersion correction) implemented in MOPAC2016.[35,36] Thereafter, the minimal energy conformer was optimized at the density functianol theory (DFT) level employing the PBE0 functional with the 6-311++G** basis set, Onsager radius and ground state dipole moments were calculated in vacuum.[37,38]

The geometries of **2** were optimized at fixed dihedral angles (Φ) (Fig. 1) for the investigation of the TICT process in vacuum using the 6-31++G** basis set with the same functional. The excited state energies were calculated the same way at the time-dependent DFT (TD-DFT) level of theory.

Results and discussions

Solvatochromism in absorption and fluorescence spectra

Compound **1** has a vibrational fine structure in its absorption as well as in its emission spectra. Besides, the absorption and emission spectra are nearly mirror images, which indicates that the geometry of the vibrationally relaxed S_1 state, from where the emission occurs, is close to the ground state structure. The Stokes shift of **1** is small (3540 cm^{-1}), its value is similar as for the parent 1,8-naphthalimide.[39]

The excited state properties of *N*-propyl-1,8-naphthalimide are strongly modified by the piperidinyl substitution. As can be seen in Fig. 2, the longest wavelength absorption band of **1**, appearing at 331 nm shifts strongly to the red, to 405 nm in the spectrum of **2**, indicating that the lowest energy excited state is stabilized due to a strong coupling of the electronic structures of the piperidinyl and 1,8-naphthalimide moieties. The electron donating piperidine substituent increases the difference between the S_0 and S_1 state energy levels: the fluorescence band located at 375 nm in the spectrum of **1** shifts to 535 nm in the spectrum of **2**. The corresponding Stokes shifts are 3540 cm^{-1} for **1** and 6000 cm^{-1} for compound **2**.

The solvatochromic behavior of the compounds was investigated in a homologous series of nitriles, minimizing the effect of the solvent specific interactions on the results. The spectral data of **1** and **2** in the nitrile solvents, and the dipole moment changes obtained from the Lippert–Mataga equation – eqn (1) – are collected in Table 1, the Lippert–Mataga plot is shown in Fig. 3 These results demonstrate that **1** is not a charge transfer dye, whereas the radiative excited state of **2** has a moderate charge transfer character. The fluorescence quantum yield of **2** grows with the decrease of the polarity, suggesting that in addition to its moderately polar emissive CT state, **2** has a more polar, but dark state and the deactivation of the CT state *via* this dark state is more efficient in solvents of higher polarity.

Effect of viscosity on fluorescence spectrum

An indication for the TICT character of this dark state was provided by the fluorescence spectra of **2** in EG at different temperatures. As can be seen in Fig. 4, the fluorescence intensity strongly decreased at higher temperatures, *i.e.* at lower viscosities, but the shape of the spectra did not change. This can arise from

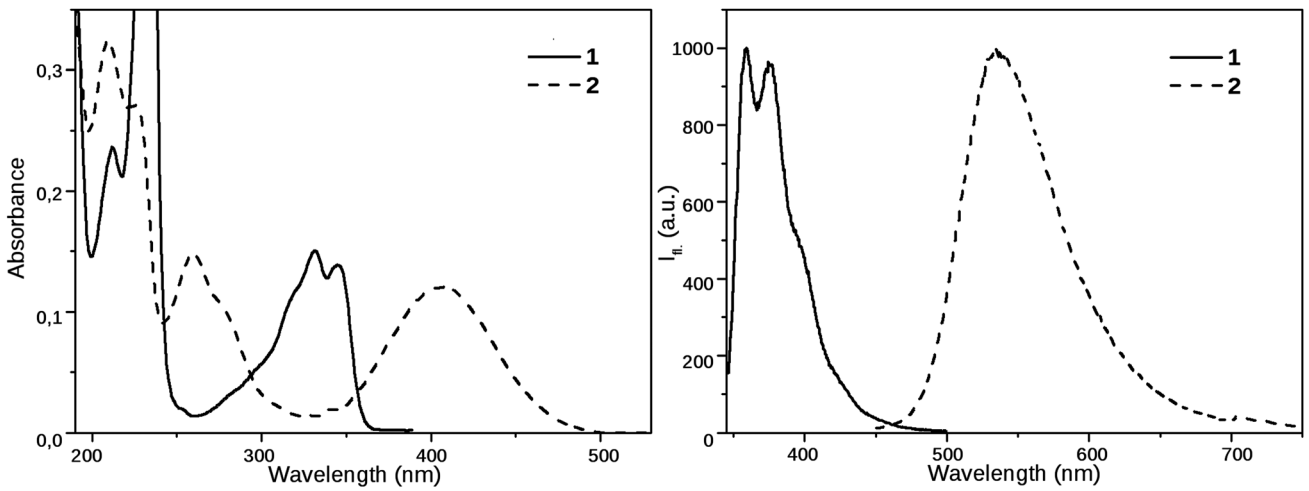

Fig. 2 Steady state absorption and emission spectra of **1** and **2** in MeCN (emission spectra were recorded using excitation at 330 nm and 405 nm, respectively).

Open Access Article. Published on 28 March 2018. Downloaded on 2/9/2026 10:35:42 PM.
This article is licensed under a Creative Commons Attribution 3.0 Unported Licence.

Table 1 Spectral properties of **1** and **2** in the homologous series of nitriles, their Onsager radius, ground state dipole moments (calculated theoretically) and dipole moment changes obtained from the Lippert–Mataga analyses

		Solvents							
		MeCN	EtCN	PrCN	BuCN	HepCN	a_0 (Å)	μ_g (D)	$\Delta\mu$ (D)
1	$\lambda_{abs}/\lambda_{em}$ (nm)	331/375	332/375	332/379	332/374	332/374	4.65	3.91	5.35
	Fl. quant. yield	0.023	0.017	0.013	0.012	0.015			
2	$\lambda_{abs}/\lambda_{em}$ (nm)	405/535	405/532	405/529	404/525	404/524	5.74	7.52	10.4
	Fl. quant. yield	0.043	0.069	0.11	0.17	0.32			

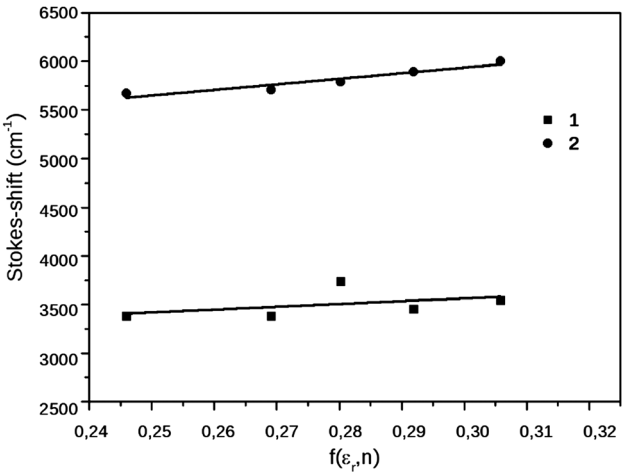

Fig. 3 Lippert–Mataga plot of **1** and **2** in the homologous series of nitriles.

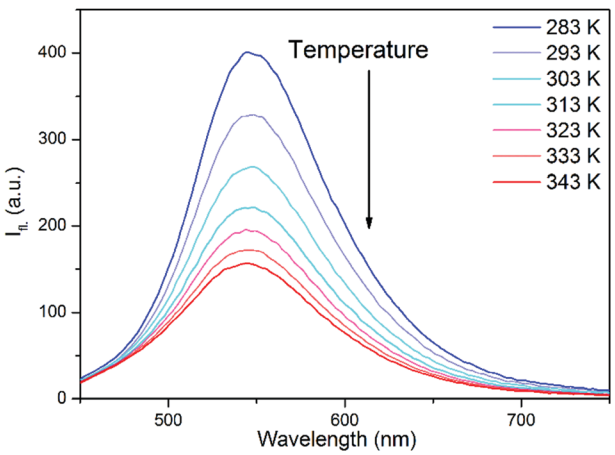

Fig. 4 Fluorescence spectra of **2** in EG at different temperatures. Excitation wavelength is 410 nm.

a deactivation channel *via* a dark TICT species, and the twist of the piperidine moiety is favored at low viscosities. The fluorescence spectrum of **1** in EG (not shown here) was much less sensitive to the temperature.

Fluorescence decay dynamics as functions of polarity and viscosity

A further insight into the excited state processes in the two NIs were performed by time resolved fluorescence experiments. The effect of polarity on the excited state dynamics was investigated in the same series of nitriles as applied in the steady-state measurements. In addition, in case of **2**, the TICT character of the non-radiative decay was studied by measuring the fluorescence decay curves in ethylene glycol (EG), at different temperatures between 10 and 70 °C, where the viscosity decreases from 34.8 to 4.0 cP, promoting the twist of the piperidine moiety. We note that the raise of temperature also has – a minor – opposite effect on the formation of the TICT state, as the polarity of EG decreases and that variation hinders the charge transfer process.

The piperidine substituted derivative **2** showed a biexponential decay in the nitrile solvents (Table 2), as well as in EG (Table 3), whereas the reference compound **1** showed biexponential decays in the nitriles and monoexponential decays

Table 2 Fitted amplitudes (A) and fluorescence lifetimes (τ) in alkyl nitriles. Emission wavelengths are 370 nm (**1**) and 540 nm (**2**)

	MeCN		EtCN		PrCN		BuCN		HepCN	
	A (%)	τ (ns)	A (%)	τ (ns)	A (%)	τ (ns)	A (%)	τ (ns)	A (%)	τ (ns)
1	99.0	0.151	99.6	0.093	99.7	0.083	99.5	0.092	99.5	0.097
	1.0	1.073	0.4	1.357	0.3	1.404	0.5	1.441	0.5	1.455
2	97.2	1.261	82.0	2.387	82.1	3.477	52.4	3.272	100.0	6.260
	2.8	8.371	18.0	3.475	17.9	4.727	47.6	4.411		

Table 3 Fitted amplitudes (A) and fluorescence lifetimes (τ) in EG at different temperatures. Emission wavelengths are 370 nm (**1**) and 540 nm (**2**)

Temperature (K)	Viscosity[40] (cP)	Dielectric constant[41] (—)	**1**		**2**	
			A (%)	τ (ns)	A (%)	τ (ns)
283	34.8	43.5	100.0	1.329	0.8	6.508
					99.2	0.143
293	22.0	41.3	100.0	1.218	1.1	6.477
					98.9	0.107
303	14.5	39.3	100.0	1.057	0.8	6.446
					99.2	0.083
313	10.0	37.3	100.0	0.944	0.8	6.355
					99.2	0.071
323	7.2	35.4	100.0	0.844	0.7	6.315
					99.3	0.060
333	5.3	33.6	100.0	0.750	0.8	6.260
					99.2	0.056
343	4.0	31.9	100.0	0.680	0.9	6.233
					99.1	0.052

This journal is © the Owner Societies 2018

Open Access Article. Published on 28 March 2018. Downloaded on 2/9/2026 10:35:42 PM.
This article is licensed under a Creative Commons Attribution 3.0 Unported Licence.

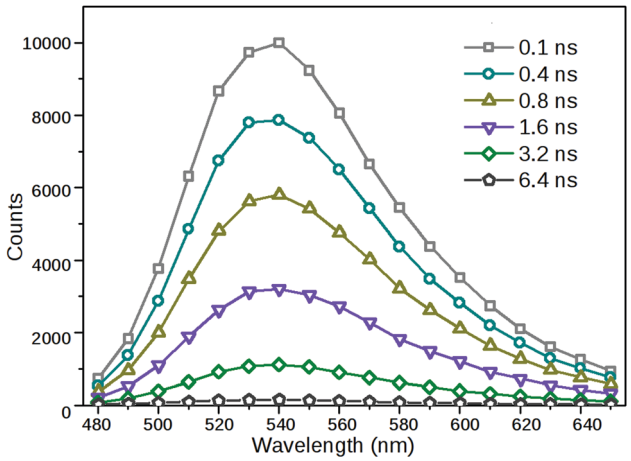

Fig. 5 Time-resolved fluorescence spectra of **2** in MeCN. Excitation wavelength is 410 nm.

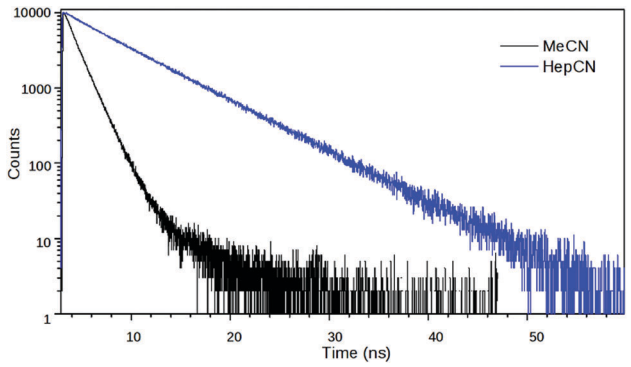

Fig. 6 Fluorescence decay curves of **2** in MeCN and HepCN at 540 nm.

in EG. In the case of **2**, the decay curves were recorded at five different wavelengths (500, 520, 540, 570, 600 nm) in all the solvents applied. The curves could be well fitted by the same time constants and relative amplitudes, which means that only a single radiative excited species had been detected.

As a further demonstration that a single radiative species had been formed *via* excitation, time-resolved fluorescence spectra of **2** were acquired from decay traces measured at different emission wavelengths. As can be seen in Fig. 5, the shapes and positions of the fluorescence bands obtained at different delay times were identical, only their relative intensities were different.

The fitted lifetime data in the nitriles show that the decay kinetics of **2** is affected more strongly by the solvent polarity than the kinetics of **1** (Table 2 and Fig. 6). The relative weights of the slow components in the decays increase with decreasing solvent polarity which is a further signal that the non-radiative state of **2** has a much stronger charge transfer character than the radiative one. Besides, the measurements in EG at different temperatures show that the excited state kinetics of **2** is influenced by the solvent viscosity. The fast component accelerates at higher temperatures, *i.e.* at lower viscosities, supporting the hypothesis that the non-radiative state is a TICT state (Fig. 7).

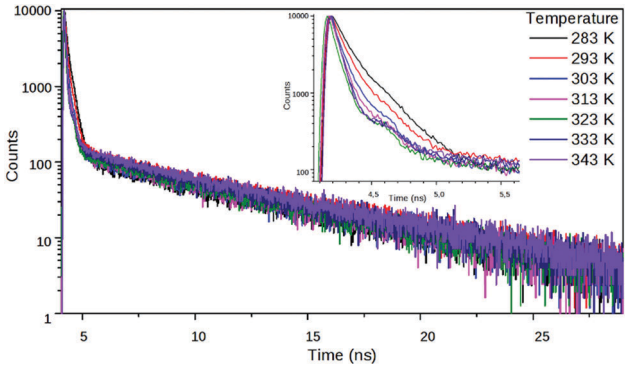

Fig. 7 Fluorescence decay curves of **2** in EG at different temperatures at 540 nm.

Kinetic analysis

Our experimental observations on the piperidino derivative **2** are consistent with the kinetic model shown in Scheme 1.

The rates can be determined using the first order differential equation system

$$\frac{\mathrm{d}\underline{c}(t)}{\mathrm{d}t} = \underline{\underline{K}}\underline{c}(t) \tag{4}$$

where $\underline{\underline{K}}$ is a matrix of the rate coefficients,

$$\underline{\underline{K}} = \begin{pmatrix} -k_x & k_{-1} \\ k_1 & -k_y \end{pmatrix},$$

with

$$k_x = k_\mathrm{C} + k_1 \tag{5}$$

$$k_y = k_\mathrm{T} + k_{-1}, \tag{6}$$

and $\underline{c}(t)$ is the vector of the concentrations as functions of time,

$$\underline{c}(t) = \begin{pmatrix} c_\mathrm{C}(t) \\ c_\mathrm{T}(t) \end{pmatrix}$$

the indices C and T refer to the excited state species CT and TICT, respectively.

Integrating eqn (4) with respect to the time we get,

$$\underline{c}(t) = \exp\left(\underline{\underline{K}}t\right)\underline{c}_0 \tag{7}$$

where $\underline{c}_0$ is the concentration vector at $t = 0$.

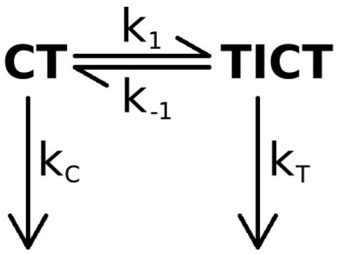

Scheme 1 The proposed kinetic scheme for the excited state processes of **2**.

Open Access Article. Published on 28 March 2018. Downloaded on 2/9/2026 10:35:42 PM.
This article is licensed under a Creative Commons Attribution 3.0 Unported Licence.

The fluorescence lifetimes, τ_1 and τ_2 are the negative reciprocals of the eigenvalues of the $\underline{\underline{K}}$ matrix, λ_1 and λ_2,

$$-\frac{1}{\tau_{1,2}} = \lambda_{1,2} = \frac{-k_x - k_y \mp \sqrt{4k_1k_{-1} + k_x^2 - 2k_xk_y + k_y^2}}{2} \quad (8)$$

The integrated forms of the rate equations are[42]

$$\begin{aligned} c_C(t) &= \left(\frac{-k_x - \lambda_2}{\lambda_1 - \lambda_2}e^{\lambda_1 t} + \frac{k_x + \lambda_1}{\lambda_1 - \lambda_2}e^{\lambda_2 t}\right)c_{0,C} \\ &= \left(a_{C,1}e^{-t/\tau_1} + a_{C,2}e^{-t/\tau_2}\right)c_{0,C} \end{aligned} \quad (9)$$

and

$$\begin{aligned} c_T(t) &= \left(\frac{k_1}{\lambda_1 - \lambda_2}e^{\lambda_1 t} - \frac{k_1}{\lambda_1 - \lambda_2}e^{\lambda_2 t}\right)c_{0,C} \\ &= a_T\left(e^{-t/\tau_1} - e^{-t/\tau_2}\right)c_{0,C} \end{aligned} \quad (10)$$

which can be obtained expanding eqn (7) by calculating the matrix exponential and assuming that $c_{0,T} = 0$.

The TICT species is non-fluorescent in the present case. The time constants τ_1 and τ_2 in eqn (9) are provided by the fitting of the decay curves to biexponential functions, the ratio of $a_{c,1}$ and $a_{c,2}$ can be obtained as the ratio of the relative amplitudes of the two decay components (pairs of A values in Tables 2 and 3),

$$\frac{a_{C,1}}{a_{C,2}} = \frac{-k_x - \lambda_2}{k_x + \lambda_1} = \frac{A_{C,1}}{A_{C,2}}. \quad (11)$$

Of the four rate coefficients in Scheme 1, k_C can be determined directly, measuring the fluorescence decay of the CT species in a frozen solvent glass.

k_x can be calculated by eqn (11), from the time constants $\tau_1(=-1/\lambda_1)$, $\tau_2(=-1/\lambda_2)$ and amplitudes of the biexponential decay curves. Using that

$$\lambda_1 + \lambda_2 = -k_x - k_y, \quad (12)$$

k_y can be calculated as well. In the possession of the values of k_C and k_x, k_1 can be obtained from eqn (5). Thereafter k_{-1} can be calculated, expressing it from eqn (8),

$$\begin{aligned} k_{-1} &= \frac{k_xk_y + k_x\lambda_1 + k_y\lambda_1 + \lambda_1^2}{k_1} \\ &= \frac{k_xk_y + k_x\lambda_2 + k_y\lambda_2 + \lambda_2^2}{k_1} \end{aligned} \quad (13)$$

Finally k_T can be calculated from eqn (6).

In a 4 : 1 EtOH : MeOH solvent mixture, **2** had a biexponential decay – with time constants (relative amplitudes) of 7.79 ns (1.4) and 0.188 ns (98.6) – whereas it had a monoexponential decay with a time constant of 9.68 ns at 77 K in frozen solvent glass where the turning of the piperidine unit is hampered so the TICT state cannot form (Fig. 8). The reciprocal of the latter lifetime was accepted as the value of k_C. Subsequently, k_1, k_{-1} and k_T were calculated from the time constants and amplitudes, following the method described above.

As can be seen in Tables 4 and 5, k_1 decreases with the decreasing solvent polarity and with increasing viscosity as is expected for a TICT state formation. Moreover, the k_T rate coefficient shows only a minor sensitivity to the solvent polarity and is insensitive to the solvent viscosity.

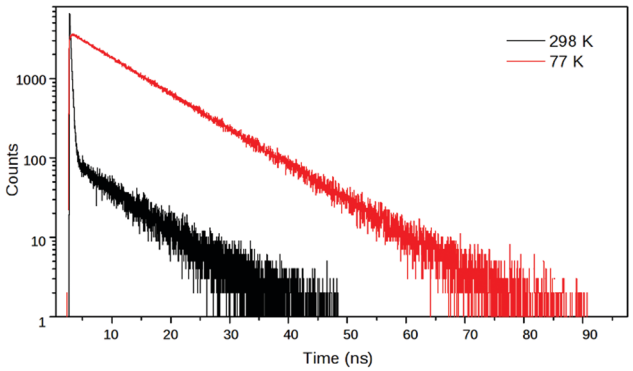

Fig. 8 Fluorescence decay curves of 2 at λ_{em} = 540 nm in EtOH : MeOH (4 : 1) at room temperature and at 77 K in frozen solvent glass.

Table 4 Rate constants for the excited state pathways of **2** in EG

Temperature (K)	k_1 (ns^{-1})	k_{-1} (ns^{-1})	k_T (ns^{-1})
283	6.8	0.053	0.15
293	9.2	0.10	0.15
303	12	0.091	0.16
313	14	0.11	0.16
323	16	0.12	0.16
333	18	0.14	0.16
343	19	0.16	0.16

The simple Arrhenius plot of the k_1–s, the rate coefficients of the CT → TICT process obtained in EG, shown in Fig. 9, is nonlinear, suggesting that the effect of the viscosity should be taken in account. The ratio of k_1/k_{-1}, which can be considered the equilibrium constant of the excited state reaction, did not change significantly, which can be because the dielectric constant of EG changed only from 44 to 32.

We can rule out that the non-linearity of the Arrhenius plot is related to solvent relaxation processes since the longitudinal relaxation time constant of EG at room temperature is around 10 ps,[43,44] whereas the k_1 rate coefficient at 293 K (9.2 ns^{-1}) corresponds to a CT → TICT conversion slower by one order of magnitude. The effects of the viscosity and polarity on the reaction rate were taken into account by taking the activation energy as the sum of three contributions,[45]

$$E_a \approx E_0 + E_{visc} + E_{pol} \quad (14)$$

where E_0 is the intrinsic barrier, E_{visc} is the effect of viscosity and E_{pol} is the effect of the polarity on the Arrhenius type barrier. Thus, the non-linearity of the Arrhenius plot can

Table 5 Rate constants for the excited state pathways of **2** in the series of nitriles

		Solvents			
		MeCN	EtCN	PrCN	BuCN
2	k_1 (ns^{-1})	0.671	0.292	0.171	0.165
	k_{-1} (ns^{-1})	0.018	0.009	0.005	0.009
	k_T (ns^{-1})	0.120	0.303	0.220	0.255

This journal is © the Owner Societies 2018

Open Access Article. Published on 28 March 2018. Downloaded on 2/9/2026 10:35:42 PM.
This article is licensed under a Creative Commons Attribution 3.0 Unported Licence.

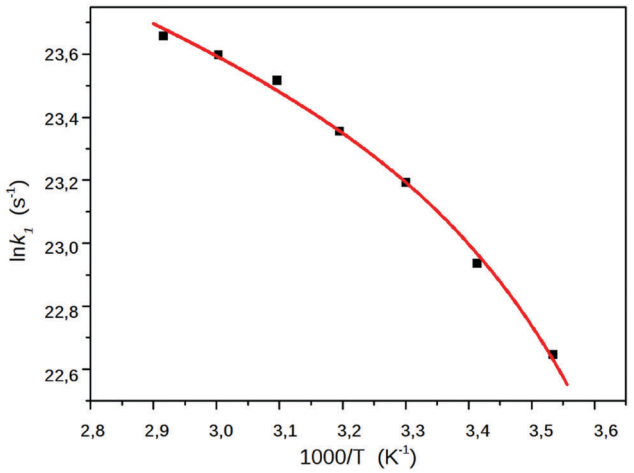

Fig. 9 The Arrhenius plot of k_1, the rate coefficient of the CT → TICT process in EG. The squares denote the experimentally determined k_1 values, the red line represents a least square fitting to eqn (19).

originate from the temperature dependency of the second two contributions in eqn (14).

The term E_{visc} was assumed as the energy of a disk rotating in a viscous fluid,[46]

$$E_{visc}(T) \approx \eta(T)b = 2\pi\eta(T)\int_0^R r^2\frac{\partial v}{\partial z}\Delta\Phi dr \qquad (15)$$

where η is the dynamic viscosity, T is the temperature, the integral multiplied by 2π was considered constant and denoted by b. The radius of the disc (piperidinyl group) is denoted with r, v is a velocity component, z is a polar coordinate (the axis of rotation) and Φ is the defined dihedral angle (see Fig. 1). E_{visc} changes rapidly in the temperature range of the kinetic experiments: its value at 343 K is only 11% of the value at 283 K.

The third term in eqn (14) was considered as the solvation energy excess of **2** at the transition state (TS) in the CT-TICT reaction,

$$E_{pol}(T) = E_{solv,TS}(T) - E_{solv,CT}(T) \qquad (16)$$

The solvation energies were estimated using the Onsager-model, according which the energy of a solute with a dipole, μ, interacts with the Onsager reaction field, R, in a spherical cavity,[47]

$$E_{solv} = -\frac{1}{2}\mu R, \qquad (17)$$

where the reaction field is calculated as

$$R = \frac{2[\varepsilon(T)-1]\mu}{[2\varepsilon(T)+1]a^3}. \qquad (18)$$

ε in eqn (18) denotes the dielectric constant and a is the Onsager radius.

The dipole moments of the CT and the TS species were calculated at the TD-DFT level (Fig. 10, 45° and −5°, respectively). The value of E_{pol} was calculated with these dipole moments at the lowest and highest temperatures applied

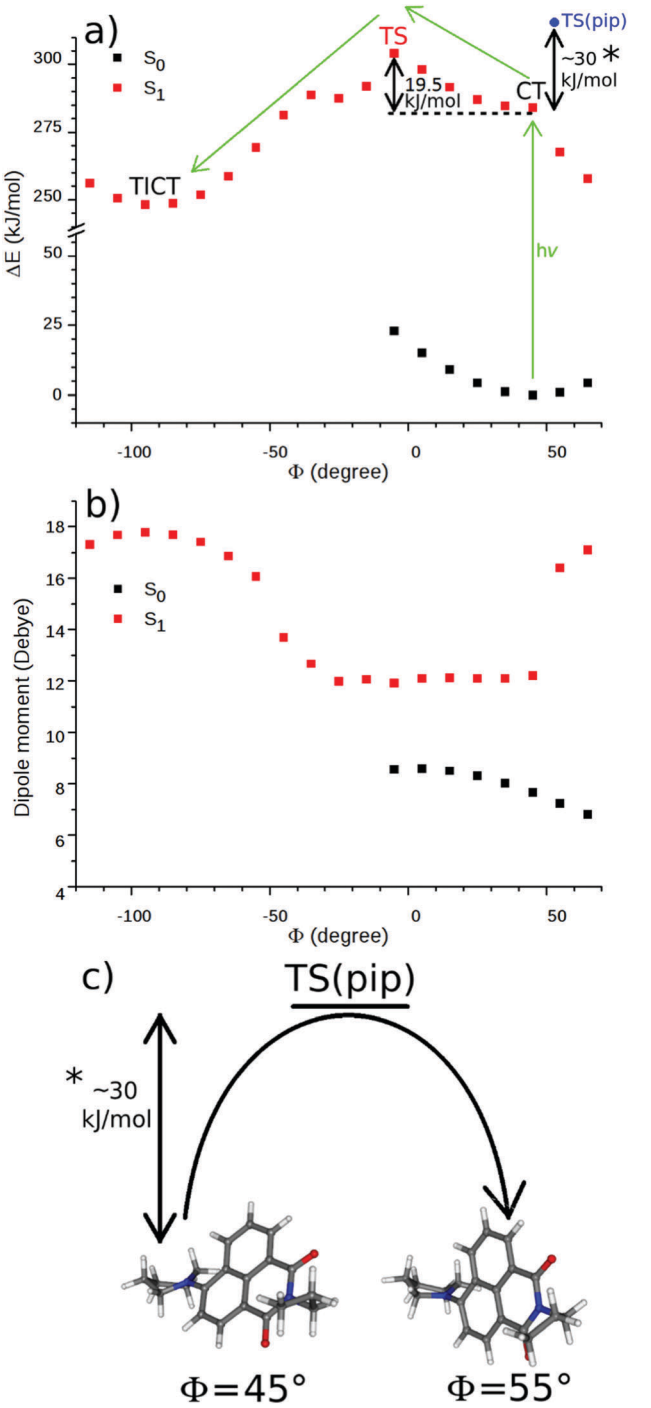

Fig. 10 Theoretical results of **2** calculated at DFT/TD-DFT level along the dihedral angle – Φ – in vacuum, (a) potential curve (the proposed reaction path is denoted with green arrows), (b) dipole moments, (c) the boat → chair transformation of the piperidine unit.

in the experiments (283 and 343 K) and only a difference of ~0.2 kJ mol^{-1} was obtained. Therefore, the temperature dependence of this term was neglected and the Arrhenius equation was written in the

$$\ln k = \frac{-E_0 - E_{pol}}{RT} + \frac{-\eta(T)b}{RT} + \ln A \qquad (19)$$

Open Access Article. Published on 28 March 2018. Downloaded on 2/9/2026 10:35:42 PM.
This article is licensed under a Creative Commons Attribution 3.0 Unported Licence.

form, where R is the gas constant and b (in J (cP mol)$^{-1}$) depends on the shape of the turning unit and also on the angle and angular velocity of the rotation.

As can be seen in Fig. 9, a nice fitting can be achieved by introducing the viscosity dependence in the kinetic barrier with the use of the expression (19). The values of the parameters of the function shown in the graph are $\ln A$ = 26.07, $E_0 + E_{pol}$ = 6.64 kJ mol^{-1} and b = 0.0415 kJ (cP mol)$^{-1}$.

Quantum chemical calculations

The theoretical calculations were performed at the DFT and the TD-DFT levels to explore the mechanism of the TICT formation of **2** further. The S1 state optimization starting from the ground state structure resulted in a similar structure with only a minor change of the dihedral angle (from 46.1° to 43.7°) and with an increase of the dipole moment from 7.6 D to 12.2 D. The latter value is close to the experimental dipole moment of *N*-butyl-4-butylamino-1,8-naphthalimide in excited state.[16] This structure represents the CT state of **2**, the existence of which was proved experimentally by the solvatochromism of this naphthalimide derivative, shown in nitriles of different polarities.

The potential curves were calculated in vacuum, along the dihedral angle between the piperidinyl moiety and the naphthalimide ring system at the DFT/TD-DFT level. Φ was changed by 10° in each step. The TICT state – the minimum on the S_1 surface – was identified at a Φ of −88° with a dipole moment of 17.7 D (see Fig. 10a and b). Its dark state property was confirmed by the TD-DFT calculation which resulted in a zero oscillator strength for the corresponding $S_1 \rightarrow S_0$ vertical transition. In contrast, the CT state proved emissive also by the calculations, an oscillator strength of 0.224 was obtained for the vertical $S_1 \rightarrow S_0$ deexcitation from the relaxed CT state.

As can be seen in Fig. 10a, the energy falls monotonously in the direction of the larger Φ angles (for the direction of the rotation see Fig. 1), which may suggest a barrierless process. A comparison of the optimized structures with fixed dihedral angles, however, reveals that there is a chair → boat conformational change of the piperidinyl unit at Φ = 55° (Fig. 10c). Probably, this arises from the repulsion of the H atoms at the bond between the piperidinyl and 1,8-naphthalimide moieties. A similar excited state folding motion of the piperidinyl group was investigated in detail experimentally in the case of some piperidinyl electron donor–other acceptor systems by Verhoeven *et al.* and barriers between 29 and 33 kJ mol^{-1} were obtained.[48] In the direction of smaller Φ angles a barrier of 19.5 kJ mol^{-1} was obtained and the chair conformation of the piperidine ring was retained, suggesting that the turning is more probable in this direction. The dipole moment (see Fig. 10b) did not change significantly on the S_1 surface until Φ reached −35° then it increased rapidly to its maximum in the TICT state where three bonds around the piperidine N atom are coplanar.

Natural bond orbital analysis were performed on the stationary points of the S_1 surface (corresponding to the CT and the TICT structures) to investigate the changes in the electronic structures. In the CT state, the orbitals of the piperidine nitrogen which form the bond with the piperidine carbons, are in sp$^{2.16}$ and sp$^{2.17}$ hybridization states and the orbital forming the bond with the naphthalimide carbon is in sp$^{1.78}$ hybridization state. In the TICT state, the bonding orbitals are purely in sp^2 hybridization state (sp$^{1.98}$, sp$^{2.02}$ and sp$^{2.00}$, respectively) as a result of the planar structure. The lone pairs are in p (>99%) hybridization state in both cases.

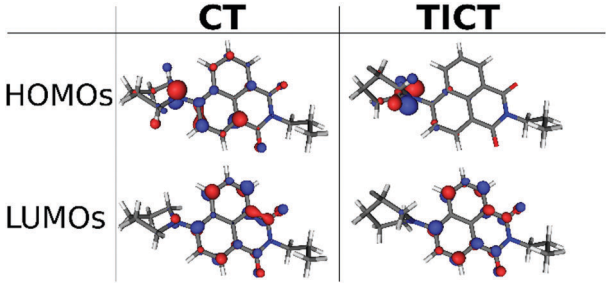

Fig. 11 The calculated molecular orbitals of the stationary points on the S_1 surface at TD-DFT level.

It is instructive to inspect the shapes of the frontier molecular orbitals (MOs) (Fig. 11). The highest occupied MO (HOMO) of the CT state is located on the nitrogen and on the aromatic naphthalimide unit in similar amounts, the LUMO primarily on the aromatic system. In the TICT state the HOMO is purely on the piperidinyl unit, the LUMO is localized mainly on the aromatic system. This result clearly demonstrates that the charge transfer is more pronounced in the TICT state which has a higher dipole moment since the excited states correspond to a completely (>97% in both cases) HOMO → LUMO excitations.

Conclusions

In this paper, an experimental proof was presented for the formation of the TICT state in a 1,8-naphthalimide based push–pull system. The fluorescence decay data were analyzed using a two state system kinetic scheme. The viscosity and polarity dependent rate constants support the hypothesis that the TICT state formation is the main quenching process of the radiative excited state, CT, of 4-piperidinyl-1,8-naphthalimide. The mono-exponential fluorescence decay in frozen solvent glass is a further evidence. A modified Arrhenius equation was employed on the excited state kinetic data in ethylene glycol which resulted in a nice fitting and in this way, we could extract the intrinsic activation energy of the TICT state formation.

The theoretical calculations show that the TICT species has a much stronger charge transfer character compared to the former CT state. Moreover, the results suggest that the turning is more likely in the direction of smaller Φ dihedral angles because there is a higher barrier of a conformational change in the other direction. Probably it is because of the repulsion of the H atoms at the bond between the piperidinyl and 1,8-naphthalimide moieties. The calculations confirm that the TICT state is dark and has a higher dipole moment compared the CT state. We hope that our results will help the development of novel 1,8-naphthalimide based molecular switches/probes and the investigation of their TICT states.

 This journal is © the Owner Societies 2018

Open Access Article. Published on 28 March 2018. Downloaded on 2/9/2026 10:35:42 PM.
This article is licensed under a Creative Commons Attribution 3.0 Unported Licence.

Conflicts of interest

There are no conflicts to declare.

Acknowledgements

Financial support for this research was provided by Hungarian NKFIH (grant K 108752), LASERLAB-EUROPE (grant agreement no. 654148, European Union's Horizon 2020 research and innovation programme), European Union MSCA-ITN-2015-ETN Action program, ISPIC, under grant no. 675743 and Netherlands Organisation for Scientific Research in the framework of the Fund New Chemical Innovation (2015) TA under grant no. 731.015.206. The computing time granted on the Hungarian HPC Infrastructure at NIIF Institute, Hungary, is gratefully acknowledged.

References

1 A. P. de Silva, H. Q. N. Gunaratne, T. Gunnlaugsson, A. J. M. Huxley, C. P. McCoy, J. T. Rademacher and T. E. Rice, *Chem. Rev.*, 1997, **97**, 1515–1566.
2 R. A. Bissell, A. P. de Silva, H. Q. N. Gunarane, P. L. M. Lynch, G. E. M. Maguire, C. P. McCoy and K. R. A. S. Sandanayake, *Top. Curr. Chem.*, 1993, **168**, 223–264.
3 G. R. C. Hamilton, S. K. Sahoo, S. Kamila, N. Singh, N. Kaur, B. W. Hyland and J. F. Callan, *Chem. Soc. Rev.*, 2015, **44**, 4415–4432.
4 A. P. de Silva, H. Q. N. Gunaratne and C. P. McCoy, *Nature*, 1993, **364**, 42–44.
5 R. M. Duke, E. B. Veale, F. M. Pfeffer, P. E. Kruger. and T. Gunnlaugsson, *Chem. Soc. Rev.*, 2010, **39**, 3936–3953.
6 D. Wang, X. Zhang, C. He and C. Duan, *Org. Biomol. Chem.*, 2010, **8**, 2923–2925.
7 J. B. Czirok, M. Bojtár, D. Hessz, P. Baranyai, L. Drahos and M. Kubinyi, I. Bitter, *Sens. Actuators, B*, 2013, **182**, 280–287.
8 G. S. Loving and B. Imperiali, *J. Am. Chem. Soc.*, 2008, **130**, 13630–13638.
9 G. S. Loving, M. Sainlos and B. Imperiali, *Trends Biotechnol.*, 2009, **28**, 73–83.
10 V. Wintgens, P. Valat, J. Kossanyi, L. Biczok, A. Demeter and T. Bérces, *J. Chem. Soc., Faraday Trans.*, 1994, **90**, 411–421.
11 V. Wintgens, P. Valat, J. Kossanyi, A. Demeter, L. Biczok and T. Bérces, *New J. Chem.*, 1996, **20**, 1149–1158.
12 E. Martín, J. L. G. Coronado, J. J. Camacho and A. Pardo, *J. Photochem. Photobiol., A*, 2005, **175**, 1–7.
13 L. Biczók, P. Valat and V. Wintgens, *Phys. Chem. Chem. Phys.*, 1999, **1**, 4759–4766.
14 S. Saha and A. Samanta, *J. Phys. Chem. A*, 2002, **106**, 4763–4771.
15 A. Pardo, J. M. L. Poyato, E. Martin, J. J. Camacho, D. Reyman, M. F. Brana and J. M. Castellano, *J. Photochem. Photobiol., A*, 1989, **46**, 323–328.
16 A. P. de Silva, H. Q. N. Gunaratne, J. L. Habib-Jiwan, C. P. McCoy, T. E. Rice and J. P. Soumillion, *Angew. Chem., Int. Ed.*, 1995, **34**, 1728–1731.
17 X. T. Jia, Y. Yang, Y. F. Xu and X. H. Qian, *Pure Appl. Chem.*, 2014, **86**, 1237–1246.
18 S. Zheng, P. L. M. Lynch, T. E. Rice, T. S. Moody, H. Q. N. Gunaratne and A. P. de Silva, *Photochem. Photobiol. Sci.*, 2012, **11**, 1675–1681.
19 P. A. Panchenko, A. N. Arkhipova, O. A. Fedorova, Y. V. Fedorov, M. A. Zakharko, D. E. Arkhipova and G. Jonusauskas, *Phys. Chem. Chem. Phys.*, 2017, **19**, 1244–1256.
20 Y. Luo, Y. Wang, S. Chen, N. Wang, Y. Qi, X. Zhang, M. Yang, Y. Huang, M. Li, J. Yu, D. Luo and Z. Lu, *Small*, 2017, **13**, e1604113.
21 F. Y. Y. Wang, W. Zhu, Y. Huang, M.-H. Yang, H. Ai and Z.-Y. Lu, *RSC Adv.*, 2014, **4**, 36849–36853.
22 T. Liu, X. Liu, D. R. Spring, X. Qian, J. Cui and Z. Xu, *Sci. Rep.*, 2014, **4**, e5418.
23 Y. Sun, X. H. Liang, J. Fan and Q. Han, *J. Lumin.*, 2013, **141**, 93–98.
24 Y. Qian, M.-M. Cai, L.-H. Xie, G.-Q. Yang, S.-K. Wu and W. Huang, *ChemPhysChem*, 2011, **12**, 397–404.
25 Y. Qian, M.-M. Cai, X.-H. Zhou, Z.-Q. Gao, X.-P. Wang, Y.-Z. Zhao, X.-H. Yan, W. Wei, L.-H. Xie and W. Huang, *J. Phys. Chem. C*, 2012, **116**, 12187–12195.
26 J.-W. Li, Y. Qian, L.-H. Xie, Y.-P. Yi, W.-W. Li and W. Huang, *J. Phys. Chem. C*, 2015, **119**, 2133–2141.
27 M. A. Landey-Alvarez, A. Ochoa-Teran, G. Pina-Luis, M. Martinez-Quiroz, M. Aguilar-Martiínez, J. Elias-Garcia, V. Miranda-Soto, J.-Z. Ramirez, L. Machi-Lara, V. L. Galvan and M. Ordonez, *Supramol. Chem.*, 2016, **28**, 892–906.
28 A. T. Peters and M. J. Bide, *Dyes Pigm.*, 1985, **6**, 349–375.
29 E. Lippert, *Z. Elektrochem.*, 1957, **61**, 962–975.
30 N. Mataga, Y. Kaifu and M. Koizumi, *Bull. Chem. Soc. Jpn.*, 1956, **29**, 465–470.
31 M. J. Frisch, G. W. Trucks, H. B. Schlegel, G. E. Scuseria, M. A. Robb, J. R. Cheeseman, G. Scalmani, V. Barone, B. Mennucci, G. A. Petersson, H. Nakatsuji, M. Caricato, X. Li, H. P. Hratchian, A. F. Izmaylov, J. Bloino, G. Zheng, J. L. Sonnenberg, M. Hada, M. Ehara, K. Toyota, R. Fukuda, J. Hasegawa, M. Ishida, T. Nakajima, Y. Honda, O. Kitao, H. Nakai, T. Vreven, J. A. Montgomery, Jr., J. E. Peralta, F. Ogliaro, M. Bearpark, J. J. Heyd, E. Brothers, K. N. Kudin, V. N. Staroverov, R. Kobayashi, J. Normand, K. Raghavachari, A. Rendell, J. C. Burant, S. S. Iyengar, J. Tomasi, M. Cossi, N. Rega, J. M. Millam, M. Klene, J. E. Knox, J. B. Cross, V. Bakken, C. Adamo, J. Jaramillo, R. Gomperts, R. E. Stratmann, O. Yazyev, A. J. Austin, R. Cammi, C. Pomelli, J. W. Ochterski, R. L. Martin, K. Morokuma, V. G. Zakrzewski, G. A. Voth, P. Salvador, J. J. Dannenberg, S. Dapprich, A. D. Daniels, Ö. Farkas, J. B. Foresman, J. V. Ortiz, J. Cioslowski and D. J. Fox, *Gaussian 09, Revision C*, Gaussian, Inc., Wallingford CT, 2009.
32 J. B. Birks, *J. Res. Natl. Bur. Stand., Sect. A*, 1976, **80**, 389–399.
33 M. J. Adams, J. G. Highfield and G. F. Kirkbright, *Anal. Chem.*, 1977, **49**, 1850–1852.
34 *MarvinSketch 16.4.25*, ChemAxon, 2016, http://chemaxon.com.
35 J. J. P. Stewart, *MOPAC2016*, Stewart Computational Chemistry, Colorado Springs, CO, USA, 2016, http://OpenMOPAC.net.

Open Access Article. Published on 28 March 2018. Downloaded on 2/9/2026 10:35:42 PM.
This article is licensed under a Creative Commons Attribution 3.0 Unported Licence.

36 J. Řezáč and P. Hobza, *J. Chem. Theory Comput.*, 2012, **8**, 141–151.
37 J. P. Perdew, K. Burke and M. Ernzerhof, *Phys. Rev. Lett.*, 1996, **77**, 3865–3868.
38 C. Adamo and V. Barone, *J. Chem. Phys.*, 1999, **110**, 6158–6169.
39 A. Pardo, J. M. L. Poyato and E. Martin, *J. Photochem.*, 1987, **36**, 323–329.
40 A. K. Coker, *Ludwig's Applied Process Design for Chemical and Petrochemical Plants*, Elsevier, 4th edn, 2015.
41 D. R. Lide, *Handbook of chemistry and physics*, 84th edn, CRC Press, 2003.
42 R. C. Evans, P. Douglas and H. D. Burrow, *Applied Photochemistry*, Springer, 2013.
43 M. Hecht and W. R. Fawcett, *J. Phys. Chem.*, 1996, **100**, 14248–14255.
44 A. Declémy, C. Rulliére and P. Kottis, *Laser Chem.*, 1990, **10**, 413–429.
45 Z. R. Grabowski, K. Rotkiewicz and W. Rettig, *Chem. Rev.*, 2003, **103**, 3899–4031.
46 L. T. Watson and C. Y. Wang, *Phys. Fluids*, 1979, **22**, 2267–2269.
47 R. O. Watts, *Mol. Phys.*, 1974, **28**, 1069–1083.
48 B. Bleisteiner, T. Marian, S. Schneider, A. M. Brouwer and J. W. Verhoeven, *Phys. Chem. Chem. Phys.*, 2001, **3**, 5383–5392.